


Origin of Magnetization Auto-Oscillations in Constriction-Based Spin Hall Nano-Oscillators

Mykola Dvornik,^{1,*} Ahmad A. Awad,¹ and Johan Åkerman^{1,2}

¹*Department of Physics, University of Gothenburg, 412 96 Gothenburg, Sweden*

²*Materials and Nanophysics, School of ICT, KTH Royal Institute of Technology, 164 00 Kista, Sweden*

 (Received 15 February 2017; revised manuscript received 4 October 2017; published 17 January 2018)

We use micromagnetic simulations to map out and compare the linear and auto-oscillating modes in constriction-based spin Hall nano-oscillators as a function of the applied magnetic field with a varying magnitude and out-of-plane angle. We demonstrate that, for all possible applied field configurations, the auto-oscillations emerge from the localized linear modes of the constriction. For field directions tending towards the plane, these modes are of the so-called edge type, i.e., localized at the opposite edges of the constriction. By contrast, when the magnetization direction approaches the film normal, the modes transform to the so-called bulk type, i.e., localized *inside* the constriction with substantially increased precession volume, consistent with the redistribution of the magnetic charges from the edges to the top and bottom surfaces of the constriction. In general, the threshold current of the corresponding auto-oscillations increases with the applied field strength and decreases with its out-of-plane angle, consistent with the behavior of the internal field and in good agreement with a macrospin model. A quantitative agreement is then achieved by taking into account the strongly nonuniform character of the system via a mean-field approximation. Both the Oersted (Oe) field and the spin-transfer torque from the drive current increase the localization and decrease the frequency of the observed mode. Furthermore, the antisymmetric Oe field breaks the lateral symmetry, favoring the localized mode at one of the two constriction edges, particularly for large out-of-plane field angles where the threshold current is significantly increased and the edge demagnetization is suppressed.

DOI: [10.1103/PhysRevApplied.9.014017](https://doi.org/10.1103/PhysRevApplied.9.014017)

I. INTRODUCTION

It is well known that ferromagnetic insulators can be excited into strongly nonlinear magnetodynamical states by the application of sufficiently strong rf magnetic fields [1–4]. The same approach, although possible, is rather inefficient for magnetic metals, as they typically exhibit much higher magnetic losses [5,6]. However, with the emergence of spin-transfer torque (STT) [7–9], it has become possible to excite and sustain highly nonlinear, nanoscale magnetization dynamics in metals, including propagating spin waves (SWs) [10–13], localized bullets [14–16], vortices [17], and droplets [18–22]. The majority of these studies have been devoted to extended geometries, where dissipative magnetic solitons are typically nucleated by employing the negative nonlinearity [23] of the system that pushes the original ferromagnetic resonance (FMR) mode into the fundamental magnonic band gap, where the propagation of spin waves is ultimately forbidden. This results in self-localization of the magnetization dynamics in the vicinity of the spin-polarized current source.

However, patterned magnetic structures support natural confinement of the magnetization dynamics, in the form of so-called edge magnonic modes [24]. These excitations are again typically observed in the fundamental band gap, which is similar to the case of dissipative magnetic solitons. Since nanopatterned materials are at the core of the emerging spintronics-based technologies, it is essential to understand their response to the application of spin-polarized currents. Prominent examples of such systems are the so-called nanoconstriction- [25,26] and nanowire-based [27,28] spin Hall nano-oscillators (SHNOs) [29–31], where pure spin currents are injected from a heavy metal (such as Pt or W) to an adjoint ferromagnetic layer [e.g., NiFe or CoFeB]. In constrictions and wires with widths below 200 nm, the injected spin current density is sufficient to nucleate self-sustained magnetization dynamics and then drive it into a strongly nonlinear regime. In contrast to extended geometries, however, the auto-oscillations in nanowire SHNOs have been shown to emerge from the semiconfined linear modes of the bulk and edge types [27]. It was later demonstrated that the edge mode becomes further localized with an increase of its amplitude [28]. Because of the significant shrinking of the nonlinear edge mode, it shows a much-reduced linewidth, as it interacts and scatters less with other modes. This property is

*Corresponding author.
mykola.dvornik@physics.gu.se

essential for successful application of SHNOs for microwave signal generation.

Although constriction-based SHNOs show even lower linewidths and, in addition, an unprecedented ability to establish mutual synchronization over large distances and device counts in out-of-plane fields [32], their dynamics has not yet been analyzed in detail. Kendziorczyk and Kuhn [33] simulated current-driven dynamics of constriction-based SHNOs in in-plane fields and demonstrated that the auto-oscillations are strongly localized to the constriction edges, consistent with the appearance of minima in the static internal field. While this correspondence might suggest that auto-oscillations originate from the linear localized mode of the nanoconstriction, the relation between the two has not been investigated. At the same time, Awad *et al.*'s micromagnetic simulations of mutually synchronized SHNOs in close-to-perpendicular fields demonstrated that mutual synchronization is possible to establish thanks to auto-oscillation modes *inside* the constriction that further extending into the SHNO leads [32]. A detailed study of the out-of-plane angular dependence of both linear and auto-oscillating spin-wave modes in constriction-based SHNOs is hence required, both to establish their relation and investigate a possible crossover from edge to bulk localization. Here, we employ micromagnetic simulations to demonstrate the origin and spatial properties of the auto-oscillations in constriction-based SHNOs for a wide range of field magnitudes and out-of-plane angles. We show that the field dependence of the threshold current agrees quite well with a macrospin model that neglects spin-wave radiation losses; the agreement essentially becomes perfect when the macrospin model is refined using a mean-field approach. We then explicitly demonstrate that, for all field angles, the auto-oscillations emerge from the localized linear modes of the constriction. For fields tending towards the plane, these localized modes reside at the constriction edges. However, when the magnetization direction approaches the film normal, the edge modes move into the interior of the constriction, transforming into a so-called bulk type with a significantly increased volume of precession.

II. MICROMAGNETIC SIMULATIONS

Here, we simulate a stack of 6-nm Pt and 5-nm Py layers containing a round-shaped nanoconstriction having a 100-nm width, an opening angle of 22° , and a curvature radii of 50 nm, as is schematically shown in Fig. 1(a). The particular choice of sample geometry follows those already investigated experimentally in the literature. The electrical current density and the corresponding Oersted (Oe) field are simulated in COMSOL [34] assuming the full-scale Pt/Py bilayer and an electrical current of $I_{\text{ref}} = 2$ mA, while linear scaling is assumed for all other values. The Oe field and the current density are sampled at the Py and Pt sites, respectively. The data are then estimated on the rectangular

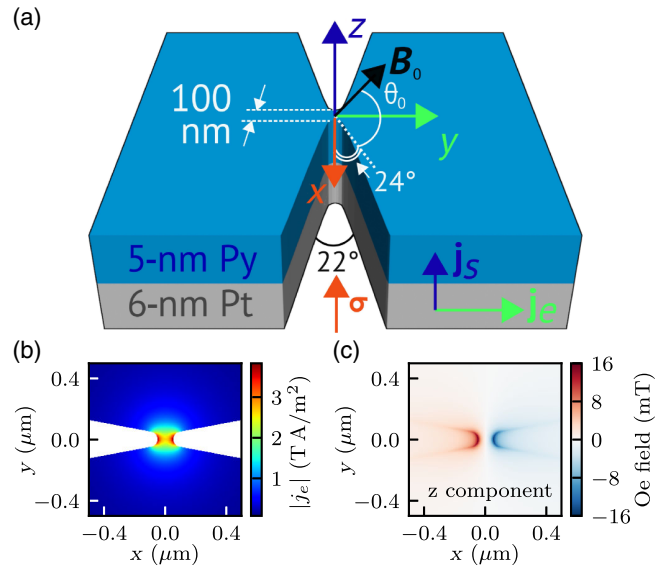


FIG. 1. (a) Schematic of the simulated Py/Pt-constriction SHNO. (b) Magnitude of the lateral electrical current density in Pt, and (b) out-of-plane component of the Oersted (Oe) field in Py calculated for an applied current of 2 mA.

mesh that is matched to the micromagnetically simulated domain. The corresponding profiles are shown in Figs. 1(b) and 1(c).

We assume that the electrical current density in Pt, \mathbf{j}_e , leads to a pure-spin-current injection into Py along the interface normal with the magnitude of $j_s = (I/I_{\text{ref}})\theta_{\text{SH}}|\mathbf{j}_e|$, where θ_{SH} is the Pt spin Hall angle and I is the applied current. Although the applied current bends in the vicinity of the constriction edges, it is still dominated by the longitudinal component (y axis). Therefore, we assume that, in accordance with the properties of the spin Hall effect, the injected spin current is uniformly polarized antiparallel to the x axis, i.e., $\boldsymbol{\sigma} = -\mathbf{x}$. We assume that the injected spin current produces a dampinglike torque of the following form [35,36]:

$$\tau_{\text{DL}} \mathbf{m} \times \boldsymbol{\sigma} \times \mathbf{m}, \quad (1)$$

where τ_{DL} and \mathbf{m} are the magnitude of the torque and reduced magnetization vector, respectively. We neglect the contributions from any Rashba fieldlike torque, as it is measured to be a few times smaller than the dampinglike one [36]. In accordance with the literature [36,37], we assume τ_{DL} to be of the Slonczewski form

$$\tau_{\text{DL}} = \frac{\gamma j_e \hbar \epsilon}{e t \mu_0 M_s}, \quad (2)$$

where M_s , γ , and t are the saturation magnetization, the gyromagnetic ratio, and the thickness of the ferromagnetic layer, respectively. The spin-polarization efficiency, ϵ , is given by

$$\epsilon = \frac{\theta_{\text{SH}}\Lambda^2}{(\Lambda^2 + 1) + (\Lambda^2 - 1)(\mathbf{m} \cdot \boldsymbol{\sigma})}, \quad (3)$$

where $\Lambda \geq 1$ is the parameter describing the transport properties of the system with respect to the relative orientation between the magnetization in the ferromagnet and the spin-current-polarization direction. In contrast to spin-transfer torque, spin-orbit torque is estimated to be practically independent of the corresponding angle [38,39], i.e., $\Lambda = 1$. Finally, we would like to point out that the experimental routine that we use to estimate a spin Hall angle of $\theta_{\text{SH}} = 0.08$ from the 10- μm -wide wires is based on the very same model.

The micromagnetic simulations are carried out using the MUMAX3 solver [40] with the input provided by the COMSOL simulations described above. Although the structure includes a heavy-metal layer, only the ferromagnetic part is explicitly considered in the simulations. The corresponding Py layer has dimensions of $2 \mu\text{m} \times 2 \mu\text{m} \times 5 \text{nm}$ subdivided into a rectangular mesh of $\Delta x \times \Delta y \times \Delta z = 3.9 \times 3.9 \times 5 \text{nm}^3$ cells. Owing to the difference in electrical resistances of the Pt and Py layers, the current mostly flows through the heavy metal. Therefore, any contribution of the current going via the ferromagnet to the magnetization dynamics, e.g., via a (nonadiabatic) spin-transfer torque, is therefore neglected in the micromagnetic simulations. The Py layer is assumed to have a saturation magnetization of $\mu_0 M_s = 0.754 \text{ T}$, a Gilbert damping of 0.02, a gyromagnetic ratio of 29.53 GHz/T, and an exchange stiffness of 10 pJ/m, as dictated by our experimental studies [32,41].

The magnetic field, B_0 , is applied at a fixed in-plane angle of 24° , which is similar to how SHNOs are typically measured [25,32]. The applied field strength, B_0 , and out-of-plane angle, θ_0 , are then varied. The magnetization dynamics is simulated by integrating the Landau-Lifshitz-Gilbert-Slonczewski equation over 187 ns, with the first 62 ns discarded in the subsequent analysis to exclude transient effects. For the sake of consistency, the linear eigenmodes of the system are estimated at the threshold current by taking into account both the Oe field and the STT. To avoid auto-oscillations, the damping of the system is increased 1.02 times, and the system is then excited by a sinc rf field with an amplitude of 1 mT and a cutoff frequency of 40 GHz. The linear response is captured over 125 ns. The frequencies and spatial profiles of linear and auto-oscillating modes of the system are extracted using methods explained elsewhere [42,43].

III. RESULTS AND DISCUSSION

For any given configuration of the applied magnetic field, we first want to estimate the auto-oscillation threshold current, I_{th} . For this purpose, at a given value of the applied current, we first run the simulations for 5 ns, where the system undergoes some transient behavior, and over the

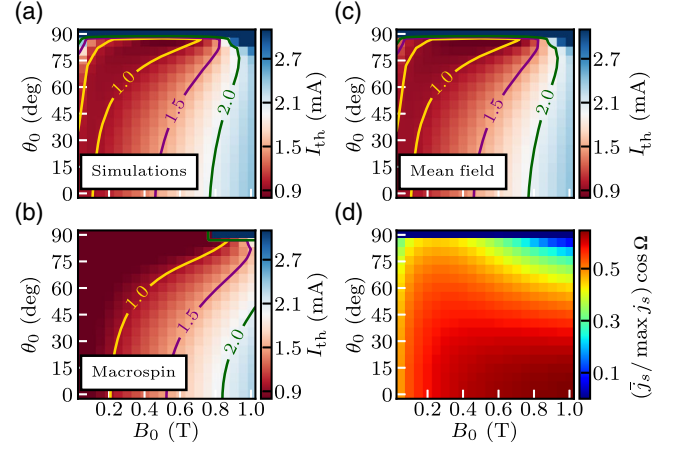


FIG. 2. Auto-oscillation threshold current vs applied field strength and out-of-plane angle as estimated (a) using micromagnetic simulations, (b) a macrospin model given by Eqs. (4) and (5), and (c) a mean-field model given by Eqs. (7) and (6). (d) The efficiency of pure-spin-current injection vs applied field geometry.

next 10 ns monitor the behavior of the maximum torque; if the maximum torque increases, we assume that auto-oscillations have started. Using this criterion, we then employ the so-called bisection method to estimate the threshold current in a range of [0.5, 5.0] mA by iteratively shrinking this interval until its bounds are separated by 1 μA , which gives $I_{\text{th}} \pm 0.5 \mu\text{A}$. Compared to the total energy, the torque shows a significantly smaller degree of numerical noise [40], which makes it more suitable for this particular type of analysis.

The results of these calculations are shown in Fig. 2(a). In general, we find that I_{th} increases with field strength and decreases with increasing field angle. This behavior can be understood using the model developed in Ref. [23]: assuming a macrospin approximation (no propagating SWs), an isotropic spin-polarization efficiency $\epsilon = 0.04$, and an easy-plane shape anisotropy, and neglecting any magneto-crystalline anisotropy, the following expression holds:

$$I_{\text{th}} = \frac{\alpha}{\sigma_0 \cos \Omega} \left(\omega_B + \frac{\omega_M}{2} \right), \quad (4)$$

where $\omega_M = \gamma \mu_0 M_s \cos^2 \theta$, $\sigma_0 = [(\epsilon \gamma \hbar) / e M_s S t]$ is the magnitude of the STT, $S = I_{\text{ref}} / \max j_s$ is the effective area of pure-spin-current injection, $\Omega = \arccos(\mathbf{m}_0 \cdot \boldsymbol{\sigma})$ is the angle between the polarization of the pure-spin current and the equilibrium magnetization direction, \mathbf{m}_0 , and θ is its out-of-plane angle. $\omega_B = \gamma B$, where B is the magnitude of the internal magnetic field, which, according to the magnetostatic boundary conditions, reads

$$B = B_0 \sqrt{1 + \frac{\mu_0 M_s}{B_0} \sin \theta \left(\frac{\mu_0 M_s}{B_0} \sin \theta - 2 \sin \theta_0 \right)}. \quad (5)$$

It follows from Eqs. (4) and (5) that the threshold current increases with the magnitude of the applied field and decreases with its out-of-plane angle, which is consistent with our simulations.

However, at high fields and large angles, which make the magnetization approach the film normal, the threshold current again increases due to (a) an increase of the internal field given by Eq. (5), and (b) a decrease of the STT efficiency as Ω approaches $\pi/2$. For applied fields close to or exceeding $\mu_0 M_s$, the out-of-plane angles of the equilibrium magnetization and the applied field increase simultaneously, so the corresponding two contributions to I_{th} counteract each other. This interplay explains the observed flattening—or even the increase—of the threshold current at high fields, and it is captured well by both simulations [Fig. 2(a)] and the macrospin model [Fig. 2(b)], which agree, at least qualitatively, in this region.

The agreement is, however, substantially worse below 0.7 T, where an increase in I_{th} is observed in the simulations despite an increase of the out-of-plane angle of the applied field and virtually no changes to the direction of the equilibrium magnetization. This discrepancy could be attributable to the reduction of the STT efficiency, e.g., due to the rotation of the magnetization in-plane, which would reduce Ω . To further examine the validity of the model given by Eq. (4), we employ a mean-field approach to estimate the relevant parameters, given by the set $\varphi = \{B, \theta, \Omega, j_s\}$, from the simulations as follows:

$$\bar{\varphi} = \frac{\sum_i \sum_j \varphi_{ij} m_{ij}^2}{\sum_i \sum_j m_{ij}^2} \quad (6)$$

where m_{ij} is the spatial profile of the auto-oscillations amplitude and the bar symbol denotes the averaged value. The summation is performed over the $500 \times 500 \text{ nm}^2$ domain around the nanoconstriction, where most of the auto-oscillation amplitude is localized. Since the spin current is strongly nonuniform, and assuming that the spatial profiles of the auto-oscillations can change with the applied field, the STT magnitude is expected to be mode specific. To account for this effect, we renormalize the STT magnitude to $\sigma'_0 = \sigma_0 \bar{j}_s / \max j_s$ and, finally, get

$$I_{\text{th}} = \frac{\gamma \alpha}{\sigma'_0 \cos \Omega} \left(\bar{B} + \frac{1}{2} \mu_0 M_s \cos^2 \bar{\theta} \right). \quad (7)$$

The data calculated using Eq. (7) are shown in Fig. 2(c). A quite remarkable *quantitative* agreement with the simulation is observed. The agreement is achieved without including any radiation losses (i.e., propagating SWs), thus confirming the localized character of the auto-oscillations, which is consistent with Refs. [25,33]. The increasing I_{th} at high out-of-plane angle and for weak applied fields is now fully recovered, which is consistent with the reduction of the pure-spin-current injection efficiency shown in

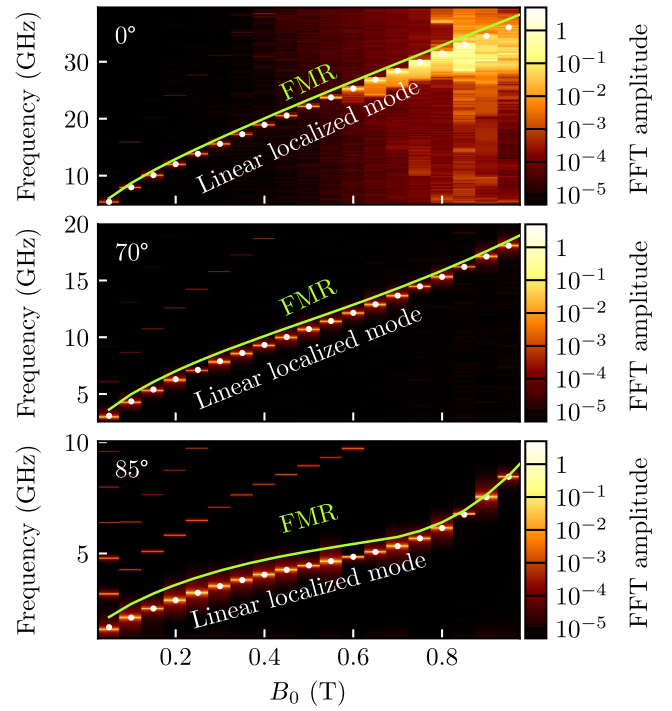


FIG. 3. Auto-oscillation spectral density vs applied field strength and three different field angles. The green lines and the white dots show frequencies of the FMR and linear localized modes, respectively.

Fig. 2(d). Specifically, we observe not only the in-plane rotation of the equilibrium magnetization, as captured by the $\cos \Omega$ term, but also the reduction of the mean-field value of the injected pure-spin-current magnitude, i.e., $\bar{j}_s / \max j_s$, which confirms changes of the auto-oscillations vs the applied field geometry.

The auto-oscillation power spectra and linear eigenmodes of the nanoconstriction, calculated at the threshold current for various field geometries, are shown in Fig. 3. The auto-oscillations always appear below the frequency of the (quasi)uniform FMR, which again confirms their localized character. However, in contrast to the extended geometries, where nonlinearity driven self-localization of the SWs happens, in our case, the auto-oscillations essentially coincide with the linear localized modes of the nanoconstriction, similarly to the nanowire SHNOs. Although our system should also support regular SW bullets, they are not observed in the simulations since the FMR amplitude is negligible inside the nanoconstriction, where most of the spin-current injection happens.

To investigate the fundamental origin of the localization, we calculate the spatial profiles of the linear modes simulated at five different applied fields and using four different combinations having the O_e field and the STT terms on or off during the simulation: Fig. 4(a) includes neither the O_e field nor STT, Fig. 4(b) includes only STT, Fig. 4(c) includes only the O_e field, and Fig. 4(d) includes both. Comparing Fig. 4(a) to Figs. 4(b)–4(d), it is clear, first

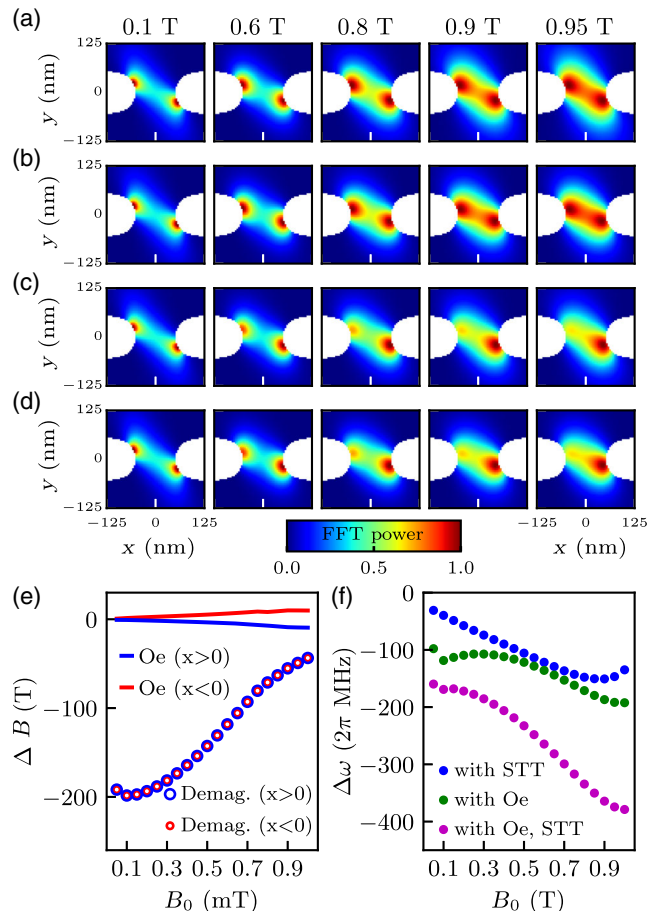


FIG. 4. Spatial profiles of the auto-oscillations calculated for a field applied at $\theta_0 = 70^\circ$ and (a) without any Oe field or STT, (b) with STT, (c) with an Oe field, and (d) with both an Oe field and STT. (e) Contribution of the demagnetizing field and the Oe field to the depth of the spin-wave wells vs the applied field strength. (f) Contribution of the STT and Oe field to the frequency of the edge mode vs the applied field strength.

of all, that neither the Oe field nor STT are required for confinement. The confinement can hence be explained by the demagnetization field alone, and the observed dynamics is essentially an edge mode typically observed in patterned magnetic structures [24] where the demagnetizing field in the vicinity of the edges creates local minima in the effective magnetic field, i.e., so-called SW wells. This field is produced by the edge magnetic charges that emerge due to the divergence of the normal-to-edge component of the equilibrium magnetization [44,45]. In our geometry, the magnetic charges on the opposite edges of the constriction arise from the divergence of the in-plane component of the equilibrium magnetization.

When we include STT, a slight reduction of the mode area is observed in strong fields [Fig. 4(b)], which is consistent with how the spin current affects the internal field. In our simulations, STT always counteracts the applied field and has its strongest contributions at the

edges, where the current density is the highest [Fig. 1(b)]. STT hence increases the depth of the SW wells and, therefore, enhances the localization of the edge modes.

The inclusion of the Oe field leads to a significant asymmetry [Fig. 4(c)] of the (otherwise symmetric) edge modes, again primarily in strong out-of-plane fields. This is a direct consequence of the antisymmetric nature of the out-of-plane component of the Oe field, with respect to the constriction center [see Fig. 1(c)]. The Oe field hence suppresses the SW well on one side of the constriction, while it strongly enhances the mode localization on the other. As both the Oe and STT contributions are proportional to the applied current, which is varied in our simulations to stay at the onset of the auto-oscillations, they are stronger in oblique fields where the threshold current is larger.

To quantify both effects, we first estimate the contributions of the demagnetizing and Oe fields to the internal field using the magnetostatic boundary conditions. Specifically, we calculate their projections on the equilibrium magnetization. If the corresponding projection is positive (negative), then it adds up to (subtracts from) the internal field; i.e., it suppresses (enhances) the SW wells. Finally, we calculate the contribution of both fields to the depth of the SW wells on the opposite edges of the constriction (i.e., $x > 0$ and $x < 0$) as $\Delta B^i = B^i(\mathbf{min}) - B^i(\mathbf{0})$, where $\mathbf{0}$ is the coordinate of the constriction center, i denotes the corresponding field contribution, and \mathbf{min} is the coordinate of the minimum in the projection of the demagnetizing field. The result is shown in Fig. 4(e).

We note that, for weak and moderate applied fields, the contribution of the Oe field is negligible compared to the demagnetization. However, at higher fields, the combined effect of (i) a weakening demagnetization due to a decreasing in-plane component of the equilibrium magnetization as it tilts out of plane, and (ii) an increasing threshold current rapidly increases the role of the Oe field. In Fig. 4(f), we finally plot how much the Oe field and STT shift the frequency of the edge mode, and we conclude that their contributions are comparable.

We now turn to the spatial profiles of the linear modes across a more complete range of field angles and strengths [Fig. 5(a)]. In most conditions, the edge mode clearly dominates and, as discussed above, remains mostly symmetric at low to moderate field strengths. At high fields and intermediate field angles, the antisymmetric influence of the Oe field is clearly visible. However, as the strength and the out-of-plane angle of the applied field increase further (i.e., towards the top-right corner of the figure), we observe a fundamental change of the spatial profile: the edge mode first localizes further, then delocalizes again, expands into the constriction, and eventually detaches from the edges to transform into a bulk mode.

This transformation is consistent with the changes in the internal field landscape shown in Fig. 6(a) and the

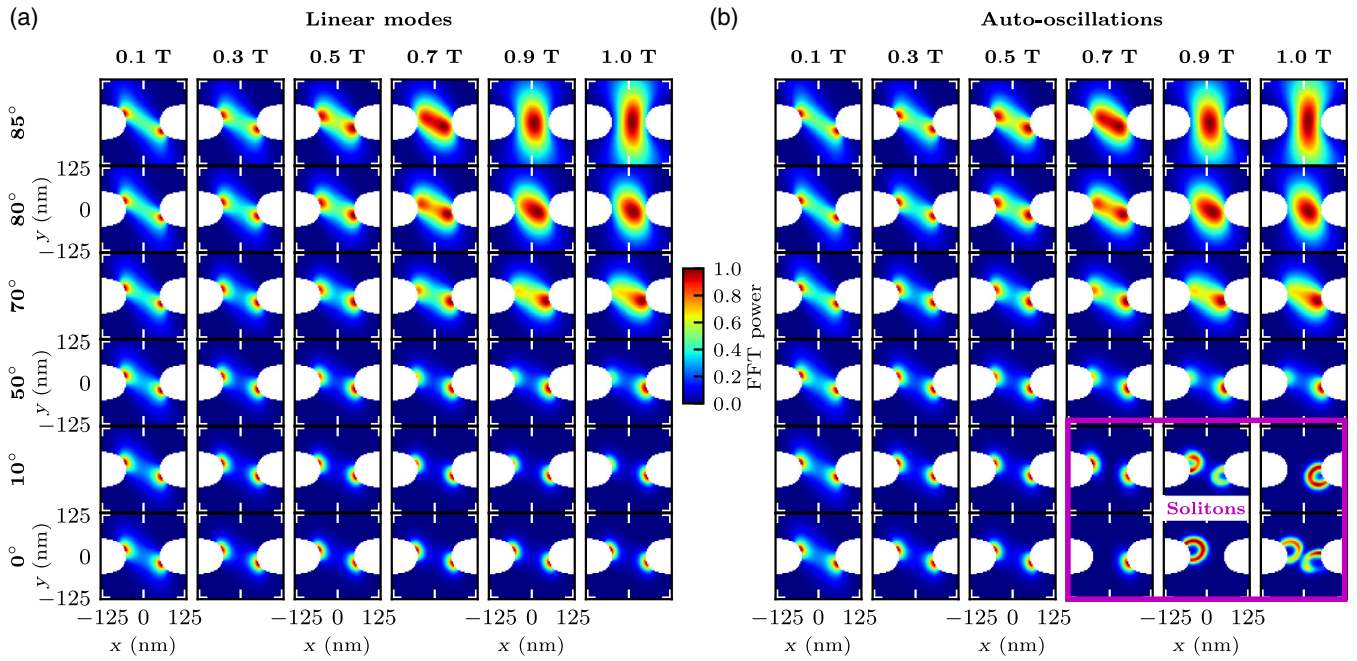


FIG. 5. Spatial profiles of the (a) linear and (b) auto-oscillating modes, simulated at unit supercriticality for applied fields with different strengths and out-of-plane angles.

reduction of the frequency gap between the FMR and the localized mode shown in Fig. 3(c). The observed behavior follows from the interplay of the magnetic charges localized on the opposite edges and (top and bottom) surfaces of the constriction, that are proportional to the magnitudes of the in-plane and out-of-plane components of the magnetization, respectively. Both components, estimated using the mean-field approach given by Eq. (6), are shown in Fig. 6(b), where we can identify three different regimes: (i) edge localization, (ii) localization in close vicinity to the edges, and (iii) bulk localization. The weakest magnetic field ($B_0 = 0.1$ T) does not saturate the sample neither out of plane nor in plane. The primarily in-plane magnetization instead bends around the constriction edges to mitigate the edge magnetic charges. The SW wells are located exactly at the edges but are not yet particularly deep, which is consistent with the relatively weak mode localization seen in the top-left corner of Fig. 5(a). When the field increases ($B_0 = 0.2$ T), the magnetization aligns more strongly with the in-plane component of the field, which increases the magnetic charge density at the edges, deepens the SW wells, and strengthens the mode localization, as seen at the bottom of Fig. 6(a).

This stronger localization is also evident from the increase of the STT efficiency shown in Fig. 2(d) for moderate fields applied over (roughly) $\theta = 60^\circ$ out of plane, as the overlap between the edge mode and the current density increases. When the field increases further ($B_0 = 0.2$ – 0.5 T), the magnetization tilts more out of plane, particularly at the edges, which gradually redistributes the magnetic charges from the constriction edges to its

surfaces. As a consequence, the SW wells detach from the edges and move gradually inward. At still higher fields ($B_0 > 0.5$ T), the surface charges dominate, the detached SW wells merge into a single shallow well closer to the constriction center, and mode localization transforms from edge to bulk.

It is now interesting to compare these linear modes with the spatial profiles of the auto-oscillations shown in Fig. 5(b). In essentially all but a few in-plane cases, the auto-oscillations are indistinguishable from the corresponding linear localized modes. In stark contrast to the extended geometries, where auto-oscillations emerge as either self-localized dissipative solitons or propagating SWs [16,18], field-localized eigenmodes can be excited for virtually any field geometry, as their existence is not dependent on the interplay of the nonlinearity and dispersion of the system.

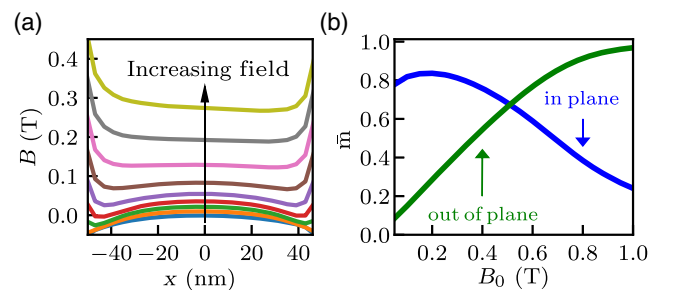


FIG. 6. (a) An effective magnetic field sampled along the constriction width vs fields applied at $\theta = 85^\circ$, ranging from 0.2 to 1 T in steps of 0.1 T. (b) Mean-field values of the in-plane and out-of-plane components of the equilibrium magnetization.

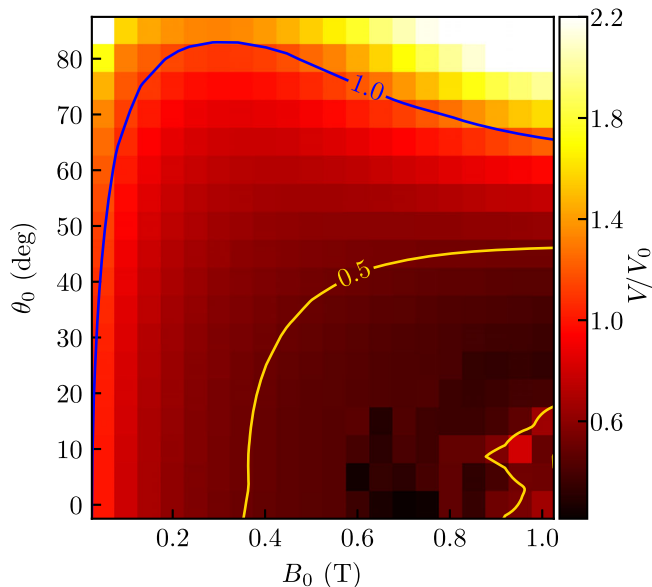


FIG. 7. Relative volume of the auto-oscillating modes vs the applied field calculated at the threshold current.

Only for strong in-plane—or very close to in-plane—fields do we observe any significant differences between the linear mode and the auto-oscillation [the violet box in Fig. 5(b)]. This deviation is also accompanied by a drop in the auto-oscillation frequency, an increase in its total power, and a much larger linewidth [see Fig. 3(a)]. However, the transient behavior of the magnetization dynamics still reveals that the auto-oscillations initially nucleate from the linear localized mode. The detailed investigation of these likely solitonic modes is, however, beyond the scope of this paper.

We finally wish to point out that, as the modes detach from the edges and move inward towards the center of the constriction, the shallow SW well allows the mode to expand quite dramatically. We can estimate the corresponding mode volume, V , using

$$V = \frac{\Delta V}{\max(m_{ij}^2)} \sum_i \sum_j m_{ij}^2,$$

where $\Delta V = \Delta x \Delta y \Delta z$ is the unit-cell volume. The relative auto-oscillation volume, V/V_0 , is shown in Fig. 7, where V_0 is obtained in the weakest in-plane field of 0.05 T. We note that V increases with the out-of-plane angle of the applied field, eventually exceeding $2V_0$ at the strongest, out-of-plane fields. This is the underlying reason that explains how robust mutual synchronization of neighboring auto-oscillating constrictions can occur [32]. We also observe that, for small-to-moderate applied field angles (i.e., below roughly $\theta_0 = 40^\circ$), the edge mode localizes further with the applied field strength, i.e., shrinks in volume. Therefore, direct coupling of the neighboring SHNOs should be vanishing in this case.

IV. CONCLUSIONS

In this paper, we demonstrate, using systematic micromagnetic simulations, that auto-oscillations in constriction SHNOs originate from the linear localized eigenmodes, which appear due to the strongly nonuniform static demagnetizing field. For fields applied mostly in plane, these modes are localized to the vicinity of the constriction edges. As the field strength and out-of-plane angle increase, the magnetic charges redistribute from the constriction edges to the surfaces, and, as a consequence, the modes change their localization character, detach from the edges, and move into the bulk of the constriction. This transformation is accompanied by a significant increase of the precession volume.

Based on a macrospin model which neglects spin-wave radiation losses, we provide a qualitative description of the auto-oscillation threshold current behavior vs the applied field. By taking into account the nonuniform character of the internal field and magnetization dynamics via a mean-field approximation, we achieve an excellent qualitative agreement with our full-scale micromagnetic simulations. In general, we observe that the stronger the localization of the edge modes, the smaller their threshold current, as (i) they experience a weaker internal magnetic field and (ii) benefit from a higher spin current density. We find that both STT and the Oe field increase the localization of the observed modes and, correspondingly, decrease their frequencies. Furthermore, the Oe field breaks the lateral symmetry of the localized modes. We believe that our results can guide the design and implementation of interacting and mutually synchronized constriction-based SHNOs, emphasizing the importance of spin-wave confinement for their operation.

ACKNOWLEDGMENTS

This work was supported by the Swedish Foundation for Strategic Research (SSF), the Swedish Research Council (VR), the Knut and Alice Wallenberg foundation (KAW), and the Wenner-Gren Foundation. This work was also supported by the European Research Council (ERC) under the European Community's Seventh Framework Programme (FP/2007–2013) and ERC Grant No. 307144 “MUSTANG.”

Note added in proof.—The authors become aware of recent work by Divinskiy *et al.* [46], who identified the solitons shown in a violet box of Fig. 5(b) to be of the magnetic droplet type.

-
- [1] P. De Gasperis, R. Marcelli, and G. Miccoli, Magnetostatic Soliton Propagation at Microwave Frequency in Magnetic Garnet Films, *Phys. Rev. Lett.* **59**, 481 (1987).

- [2] Ming Chen, Mincho A. Tsankov, Jon M. Nash, and Carl E. Patton, Microwave Magnetic-Envelope Dark Solitons in Yttrium Iron Garnet Thin Films, *Phys. Rev. Lett.* **70**, 1707 (1993).
- [3] M. Bauer, O. Büttner, S. O. Demokritov, B. Hillebrands, V. Grimalsky, Yu. Rapoport, and A. N. Slavin, Observation of Spatiotemporal Self-Focusing of Spin Waves in Magnetic Films, *Phys. Rev. Lett.* **81**, 3769 (1998).
- [4] O. Büttner, M. Bauer, S. O. Demokritov, B. Hillebrands, Yuri S. Kivshar, V. Grimalsky, Yu. Rapoport, and A. N. Slavin, Linear and nonlinear diffraction of dipolar spin waves in yttrium iron garnet films observed by space- and time-resolved Brillouin light scattering, *Phys. Rev. B* **61**, 11576 (2000).
- [5] V. E. Demidov, M. Buchmeier, K. Rott, P. Krzysteczko, J. Münchenberger, G. Reiss, and S. O. Demokritov, Nonlinear Hybridization of the Fundamental Eigenmodes of Microscopic Ferromagnetic Ellipses, *Phys. Rev. Lett.* **104**, 217203 (2010).
- [6] P. S. Keatley, P. Gangmei, M. Dvornik, R. J. Hicken, J. R. Childress, and J. A. Katine, Large amplitude magnetization dynamics and the suppression of edge modes in a single nanomagnet, *Appl. Phys. Lett.* **98**, 082506 (2011).
- [7] J. C. Slonczewski, Current-driven excitation of magnetic multilayers, *J. Magn. Magn. Mater.* **159**, L1 (1996).
- [8] L. Berger, Emission of spin waves by a magnetic multilayer traversed by a current, *Phys. Rev. B* **54**, 9353 (1996).
- [9] D. C. Ralph and M. D. Stiles, Spin transfer torques, *J. Magn. Magn. Mater.* **320**, 1190 (2008).
- [10] M. Tsoi, A. G. M. Jansen, J. Bass, W.-C. Chiang, M. Seck, V. Tsoi, and P. Wyder, Excitation of a Magnetic Multilayer by an Electric Current, *Phys. Rev. Lett.* **80**, 4281 (1998).
- [11] J. Slonczewski, Excitation of spin waves by an electric current, *J. Magn. Magn. Mater.* **195**, L261 (1999).
- [12] M. Madami, S. Bonetti, G. Consolo, S. Tacchi, G. Carlotti, G. Gubbiotti, F. B. Mancoff, M. A. Yar, and J. Åkerman, Direct observation of a propagating spin wave induced by spin-transfer torque, *Nat. Nanotechnol.* **6**, 635 (2011).
- [13] M. Madami, E. Iacocca, S. Sani, G. Gubbiotti, S. Tacchi, R. K. Dumas, J. Åkerman, and G. Carlotti, Propagating spin waves excited by spin-transfer torque: A combined electrical and optical study, *Phys. Rev. B* **92**, 024403 (2015).
- [14] W. H. Rippard, M. R. Pufall, S. Kaka, S. E. Russek, and T. J. Silva, Direct-Current Induced Dynamics in $\text{Co}_{90}\text{Fe}_{10}/\text{Ni}_{80}\text{Fe}_{20}$ Point Contacts, *Phys. Rev. Lett.* **92**, 027201 (2004).
- [15] A. Slavin and V. Tiberkevich, Spin Wave Mode Excited by Spin-Polarized Current in a Magnetic Nanocontact is a Standing Self-Localized Wave, *Phys. Rev. Lett.* **95**, 237201 (2005).
- [16] S. Bonetti, V. Tiberkevich, G. Consolo, G. Finocchio, P. Muduli, F. Mancoff, A. Slavin, and J. Åkerman, Experimental Evidence of Self-Localized and Propagating Spin Wave Modes in Obliquely Magnetized Current-Driven Nanocontacts, *Phys. Rev. Lett.* **105**, 217204 (2010).
- [17] Q. Mistral, Joo-Von Kim, T. Devolder, P. Crozat, C. Chappert, J. A. Katine, M. J. Carey, and K. Ito, Current-driven microwave oscillations in current perpendicular-to-plane spin-valve nanopillars, *Appl. Phys. Lett.* **88**, 192507 (2006).
- [18] S. M. Mohseni, S. R. Sani, J. Persson, T. N. Anh Nguyen, S. Chung, Ye. Pogoryelov, P. K. Muduli, E. Iacocca, A. Eklund, R. K. Dumas, S. Bonetti, A. Deac, M. A. Hoefer, and J. Åkerman, Spin torque-generated magnetic droplet solitons, *Science* **339**, 1295 (2013).
- [19] Ferran Macià, Dirk Backes, and Andrew D. Kent, Stable magnetic droplet solitons in spin-transfer nanocontacts, *Nat. Nanotechnol.* **9**, 992 (2014).
- [20] S. Chung, S. M. Mohseni, S. R. Sani, E. Iacocca, R. K. Dumas, T. N. Anh Nguyen, Ye. Pogoryelov, P. K. Muduli, A. Eklund, M. Hoefer, and J. Åkerman, Spin transfer torque generated magnetic droplet solitons (invited), *J. Appl. Phys.* **115**, 172612 (2014).
- [21] Sunjae Chung, S. Majid Mohseni, Anders Eklund, Philipp Dürrenfeld, Mojtaba Ranjbar, Sohrab R. Sani, T. N. Anh Nguyen, Randy K. Dumas, and Johan Åkerman, Magnetic droplet solitons in orthogonal spin valves, *Low Temp. Phys.* **41**, 833 (2015).
- [22] Sunjae Chung, Anders Eklund, Ezio Iacocca, Seyed Majid Mohseni, Sohrab R. Sani, Lake Bookman, Mark A. Hoefer, Randy K. Dumas, and Johan Åkerman, Magnetic droplet nucleation boundary in orthogonal spin torque nano-oscillators, *Nat. Commun.* **7**, 11209 (2016).
- [23] A. N. Slavin and P. Kabos, Approximate theory of microwave generation in a current-driven magnetic nanocontact magnetized in an arbitrary direction, *IEEE Trans. Magn.* **41**, 1264 (2005).
- [24] J. Jorzick, S. O. Demokritov, B. Hillebrands, M. Bailleul, C. Fermon, K. Y. Guslienko, A. N. Slavin, D. V. Berkov, and N. L. Gorn, Spin Wave Wells in Nonellipsoidal Micrometer Size Magnetic Elements, *Phys. Rev. Lett.* **88**, 047204 (2002).
- [25] V. E. Demidov, S. Urazhdin, A. Zholud, A. V. Sadovnikov, and S. O. Demokritov, Nanoconstriction-based spin-Hall nano-oscillator, *Appl. Phys. Lett.* **105**, 172410 (2014).
- [26] Hamid Mazraati, Sunjae Chung, Afshin Houshang, Mykola Dvornik, Luca Piazza, Fatjon Qejvanaj, Sheng Jiang, Tuan Q. Le, Jonas Weissenrieder, and Johan Åkerman, Low operational current spin Hall nano-oscillators based on NiFe/W bilayers, *Appl. Phys. Lett.* **109**, 242402 (2016).
- [27] Zheng Duan, Andrew Smith, Liu Yang, Brian Youngblood, Jürgen Lindner, Vladislav E. Demidov, Sergej O. Demokritov, and Ilya N. Krivorotov, Nanowire spin torque oscillator driven by spin orbit torques, *Nat. Commun.* **5**, 5616 (2014).
- [28] Liu Yang, Roman Verba, Vasil Tiberkevich, Tobias Schneider, Andrew Smith, Zheng Duan, Brian Youngblood, Kilian Lenz, Jürgen Lindner, Andrei N. Slavin, and Ilya N. Krivorotov, Reduction of phase noise in nanowire spin orbit torque oscillators, *Sci. Rep.* **5**, 16942 (2015).
- [29] Tingsu Chen, Randy K. Dumas, Anders Eklund, Pranaba K. Muduli, Afshin Houshang, Ahmad A. Awad, Philipp Dürrenfeld, B. Gunnar Malm, Ana Rusu, and Johan Åkerman, Spin-torque and spin-Hall nano-oscillators, *Proc. IEEE* **104**, 1919 (2016).
- [30] Vladislav E. Demidov, Sergej Urazhdin, Henning Ulrichs, Vasil Tiberkevich, Andrei Slavin, Dietmar Baither, Guido Schmitz, and Sergej O. Demokritov, Magnetic nano-oscillator driven by pure spin current, *Nat. Mater.* **11**, 1028 (2012).

- [31] M. Ranjbar, P. Dürrenfeld, M. Haidar, E. Iacocca, M. Balinskiy, T. Q. Le, M. Fazlali, A. Houshang, A. A. Awad, R. K. Dumas, and J. Åkerman, CoFeB-based spin Hall nano-oscillators, *IEEE Magn. Lett.* **5**, 3000504 (2014).
- [32] A. A. Awad, P. Dürrenfeld, A. Houshang, M. Dvornik, E. Iacocca, R. K. Dumas, and J. Åkerman, Long-range mutual synchronization of spin Hall nano-oscillators, *Nat. Phys.* **13**, 292 (2017).
- [33] T. Kendziorczyk and T. Kuhn, Mutual synchronization of nanoconstriction-based spin Hall nano-oscillators through evanescent and propagating spin waves, *Phys. Rev. B* **93**, 134413 (2016).
- [34] COMSOL, Inc., COMSOL MULTIPHYSICS software.
- [35] Paul M. Haney, Hyun-Woo Lee, Kyung-Jin Lee, Aurélien Manchon, and M. D. Stiles, Current induced torques and interfacial spin-orbit coupling: Semiclassical modeling, *Phys. Rev. B* **87**, 174411 (2013).
- [36] Tianxiang Nan, Satoru Emori, Carl T. Boone, Xinjun Wang, Trevor M. Oxholm, John G. Jones, Brandon M. Howe, Gail J. Brown, and Nian X. Sun, Comparison of spin-orbit torques and spin pumping across NiFe/Pt and NiFe/Cu/Pt interfaces, *Phys. Rev. B* **91**, 214416 (2015).
- [37] Luqiao Liu, Takahiro Moriyama, D. C. Ralph, and R. A. Buhrman, Spin-Torque Ferromagnetic Resonance Induced by the Spin Hall Effect, *Phys. Rev. Lett.* **106**, 036601 (2011).
- [38] Kevin Garello, Ioan Mihai Miron, Can Onur Avci, Frank Freimuth, Yuriy Mokrousov, Stefan Blügel, Stéphane Auffret, Olivier Boule, Gilles Gaudin, and Pietro Gambardella, Symmetry and magnitude of spin-orbit torques in ferromagnetic heterostructures, *Nat. Nanotechnol.* **8**, 587 (2013).
- [39] Ki-Seung Lee, Dongwook Go, Aurélien Manchon, Paul M. Haney, M. D. Stiles, Hyun-Woo Lee, and Kyung-Jin Lee, Angular dependence of spin-orbit spin-transfer torques, *Phys. Rev. B* **91**, 144401 (2015).
- [40] Arne Vansteenkiste, Jonathan Leliaert, Mykola Dvornik, Mathias Helsen, Felipe Garcia Sanchez, and Bartel Van Waeyenberge, The design and verification of MUMAX3, *AIP Adv.* **4**, 107133 (2014).
- [41] Philipp Dürrenfeld, Ahmad A. Awad, Afshin Houshang, Randy K. Dumas, and Johan Åkerman, A 20 nm spin Hall nano-oscillator, *Nanoscale* **9**, 1285 (2017).
- [42] Mykola Dvornik, Ph.D. thesis, University of Exeter, 2011, <https://ore.exeter.ac.uk/repository/handle/10036/3304>.
- [43] M. Dvornik, Y. Au, and V. V. Kruglyak, in *Magnonics: From Fundamentals to Applications*, Topics in Applied Physics Vol. 125, edited by Sergej O. Demokritov and Andrei N. Slavin (Springer Nature, New York, 2013), p. 101.
- [44] R. I. Joseph and E. Schlömann, Demagnetizing field in nonellipsoidal bodies, *J. Appl. Phys.* **36**, 1579 (1965).
- [45] Paul Bryant and Harry Suhl, Thin film magnetic patterns in an external field, *Appl. Phys. Lett.* **54**, 2224 (1989).
- [46] B. Divinskiy, S. Urazhdin, V. E. Demidov, A. Kozhanov, A. P. Nosov, A. B. Rinkevich, and S. O. Demokritov, Magnetic droplet solitons generated by pure spin currents, *Phys. Rev. B* **96**, 224419 (2017).